catalysts

MDPI

Article

Computational Redesign of Aspartase from *Escherichia coli* and Its Catalytic Synthesis of β-Alanine

Long-Xian Li, Bao-Di Ma and Yi Xu *

Faculty of Chemical Engineering and Energy Technology, Shanghai Institute of Technology, 100 Haiquan Road, Shanghai 201418, China; 216061151@mail.sit.edu.cn (L.-X.L.); mbd2966@sit.edu.cn (B.-D.M.)
* Correspondence: xuyi@sit.edu.cn; Tel.: +86-21-60873024

Abstract

Aspartase from *Escherichia coli* (AspA) catalyzes the direct conversion of acrylic acid to β-alanine; however, its substrate specificity and low catalytic efficiency limit its broader application. We engineered an AspA mutant capable of efficiently catalyzing the amination of acrylic acid for β-alanine synthesis, using Rosetta Enzyme Design to computationally redesign the Cβ-binding region of the acrylic acid binding site in AspA. Based on energy scores, structural configurations, and hydrogen bonding networks, 51 candidate variants with penalty scores below 30 were selected for mutant construction and performance testing; >70% of these variants exhibited enhanced catalytic activity in acrylic acid's hydrogen amination. Four mutants achieved over 3-fold improved activity. The optimal mutant, M1 (T190I-M324I-K327L-N329C), demonstrated a 7.3-fold increased specific enzyme activity and a 13.0-fold improved k_{cat}/K_m compared with the wild type. Conformational changes in the S-loop and enhanced hydrophobic interactions near the active site contributed significantly to M1's enhanced activity. Upon reaction optimization, the conversion of β-alanine synthesis using M1 in whole-cell catalysis increased from 5% with the wild type to 90% with M1. This study provides a reference for the biocatalytic synthesis of β-alanine, significantly enhancing the conversion of acrylic acid and demonstrating the enzyme's potential for industrial applications.

Keywords: aspartase; rational design; β-Alanine; biotransformation

1. Introduction

In nature, β-amino acids are considerably less common than α-amino acids, yet they have attracted increasing attention in recent years. β-Alanine serves as a key precursor for the synthesis of numerous substances [1]—including 3-hydroxypropionic acid [2], poly(3-hydroxypropanoate) [3], pantothenic acid [4], carnosine [5], and pamidronic acid [6]. It demonstrates broad applicability across the food, feed, pharmaceutical, and chemical industries [7–10].

Production of β-alanine primarily involves chemical synthesis, microbial fermentation, and enzymatic conversion. The chemical synthesis process, particularly the acrylonitrile method, utilizes flammable, highly toxic, and environmentally hazardous raw materials. This method also requires high temperatures and pressures, significant energy consumption, complex operations, and the generation of harmful by-products. Microbial fermentation uses low-cost raw materials but faces industrial constraints, such as competition between cell growth and enzyme expression, prolonged fermentation cycles, inhibition at high concentrations, and competing metabolic pathways [11]. Enzymatic conversion has garnered

Check for updates

Academic Editors: Evangelos Topakas, Juan M. Bolivar and Chia-Hung Kuo

Received: 1 June 2026
Revised: 13 July 2026
Accepted: 14 July 2026
Published: 16 July 2026

Copyright: © 2026 by the authors. Licensee MDPI, Basel, Switzerland. This article is an open access article distributed under the terms and conditions of the Creative Commons Attribution (CC BY) license.

attention for its short conversion cycles, high production rates, minimal by-product formation, and high product purity. Enzymatic methods are categorized into single-, double-, and triple-enzyme systems. The double-enzyme approach typically couples aspartase with L-aspartic acid-α-decarboxylase, but suffers from substrate loss, multiple reaction steps, and low yields [12].

Recently, our research group developed a triple-enzyme coupling system that achieved a 93.9% conversion using cost-effective maleic acid. However, tri-enzyme coupling poses considerable challenges owing to the disparate optimal reaction conditions required for each enzyme [13]. Accordingly, the single-enzyme method has emerged as a focal research area owing to its operational simplicity and high conversion efficiency, comprising the β-aminopropionitrile and L-aspartate pathways. The latter leverages L-aspartate α-decarboxylase for direct β-alanine synthesis, offering high yield and conversion. However, it requires substantial enzyme preparations, which raise production costs. Advancements in cost-effective, efficient enzyme preparations remain crucial for the industrialization of β-alanine production.

Directed evolution has become a widely used approach for modifying enzyme properties such as stability [14], substrate specificity [15], and selectivity [16]. In the absence of detailed structural and mechanistic information, directed evolution enables the identification of desirable mutants but often necessitates high-throughput expression platforms or extensive mutant libraries [17], which can be impractical under certain complex expression conditions [18–21]. Notably, only a few amino acid residues within an enzyme influence its catalytic function, typically within the substrate-binding pocket. Semi-rational design targets these key residues based on existing sequence, structural, and functional data, constructing a mutant library via iterative saturation mutagenesis to balance sequence diversity and screening workload. The efficacy of semi-rational design depends heavily on the depth of preliminary structural and functional information.

Rational design, another core strategy for discovering and improving enzymes [22], uses computational tools to simulate natural evolutionary processes, focusing on specific residues for virtual mutagenesis and efficient variant screening [23]. The Rosetta software suite (Rosetta3), developed by Dr. David Baker's laboratory at the University of Washington, has facilitated advances in computational biology, including de novo protein design, enzyme engineering, ligand docking, and biomolecular structure prediction. Its specialized module, Rosetta Enzyme Design, enables targeted redesign of protein–ligand complexes, facilitating the establishment of specific catalytic interactions and optimizing the configurations of adjacent residues [24]. This platform has enabled the design of enzymes for diverse reactions, including Kemp elimination [25], Retro-Aldol reactions [26], diene synthase activity [27], and the hydrolysis of organophosphorus compounds by zinc-dependent metalloenzymes [28].

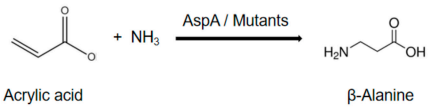
Aspartase, a member of the aminolyase family, was initially identified in several facultative aerobic bacteria and subsequently found in a broad range of organisms, including various bacteria, plants, mammals, and viruses [29]. Despite catalyzing deamination reactions, aspartases exhibit limited similarity to other amine hydrolases and feature distinct deamination mechanisms [30].

AspB, an aspartase derived from *Bacillus*, exemplifies this class: it utilizes Ser318 as a general base to abstract the pro-R hydrogen from aspartate's Cβ atom during deamination. The negative charge of the resulting enolate intermediate is stabilized through an intricate network of hydrogen bonds involving Thr101, Ser140, Thr141, Ser319, and the β-carboxylate ester group. This intermediate subsequently decomposes to yield fumarate and ammonia [31]. Previous research has highlighted key binding sites on aspartase, including T187, M321, K324, and K326 [32]. To clarify the relationship between residue

positions across homologous enzymes, a sequence alignment between AspB and *Escherichia coli* AspA was performed. The results revealed that AspB residues T187, M321, K324, and K326 correspond to AspA residues T190, M324, K327, and N329, respectively. Based on this correspondence, these positions were selected as mutation hotspots in the present study to maintain functional conservation while enabling local environment optimization. Furthermore, Wu et al. adjusted the enzyme's α-carboxylate binding pocket to accommodate alternative substituents while preserving interactions within the functional β-carboxylate binding pocket. Enhanced hydrophobic interactions between the Cβ and surrounding substrate residues further facilitated the catalytic synthesis of various β-amino acids, including those derived from crotonic acid, (*E*)-2-pentenoic acid, monoamide fumarate, and (*E*)-cinnamic acid [33].

Aspartase from *Escherichia coli* (AspA) efficiently catalyzes the synthesis of L-aspartic acid from fumaric acid. Early studies demonstrated enzymatic L-aspartate production from fumarate and ammonia using aspartase-containing immobilized *Escherichia coli* cells. Sato et al. reported that UV-induced high-yield strains enabled rapid production within 1 h, achieving rates of 0.19–0.35 g/min/g (dry cell mass). Subsequent immobilization strategies enabled continuous production with productivity reaching 6 g/h/g (dry cell mass), significantly improving industrial feasibility [34]. Aspartase catalyzes the reversible conversion between L-aspartate and fumarate with ammonia, with alkaline conditions favoring L-aspartate formation. Over decades, its crystal structure, catalytic mechanism, and biochemical properties have been widely investigated. Among various sources, *Escherichia coli* aspartase (AspA) remains the most commonly used in industrial applications due to its efficiency and cost-effectiveness.

Our previous work demonstrated AspA's capacity to catalyze the hydrogenation of acrylic acid to β-alanine [13]. Building on these findings, in the current study, we modified the loop region of the substrate-binding site—guided by structural differences between fumaric acid and acrylic acid—and computationally redesigned AspA using Rosetta enzyme design. The primary objective of the study was to engineer an AspA mutant capable of efficiently catalyzing the amination of acrylic acid for β-alanine synthesis. A highly efficient biocatalytic method for synthesizing β-alanine is presented (Scheme 1). The protein engineering strategy employed provides valuable insights for the engineering of other microbial enzymes.



Scheme 1. Aspartase-catalyzed amination of acrylic acid to β-alanine.

2. Results

2.1. Computational Redesign of Highly Active Aspartase Mutants

We first examined the reaction mechanism of AspA, supported by X-ray crystallography [29], site-directed mutagenesis [25], and quantum-chemical calculations [24]. Aspartase forces the substrate into a high-energy state. In the deamination direction, the general base Ser321 extracts the pro-R proton from the C_β atom of aspartic acid. The resulting negative charge on the acrylic acid intermediate is stabilized by a hydrogen-bond network involving Thr104, Ser143, Thr144, Ser322, and the carboxyl group. The collapse of this intermediate yields acrylic acid and ammonia. Substrate binding also involves interactions between the C_α atom and the protein environment, including Asn145, Thr190, Glu191, Met324, Lys327, and Asn329. As Asn145 and Glu191 are essential for amino acid activity, they were

excluded from mutagenesis. Therefore, Thr190, Met324, Lys327, and Asn329 were selected for simultaneous mutation (Figure 1a).

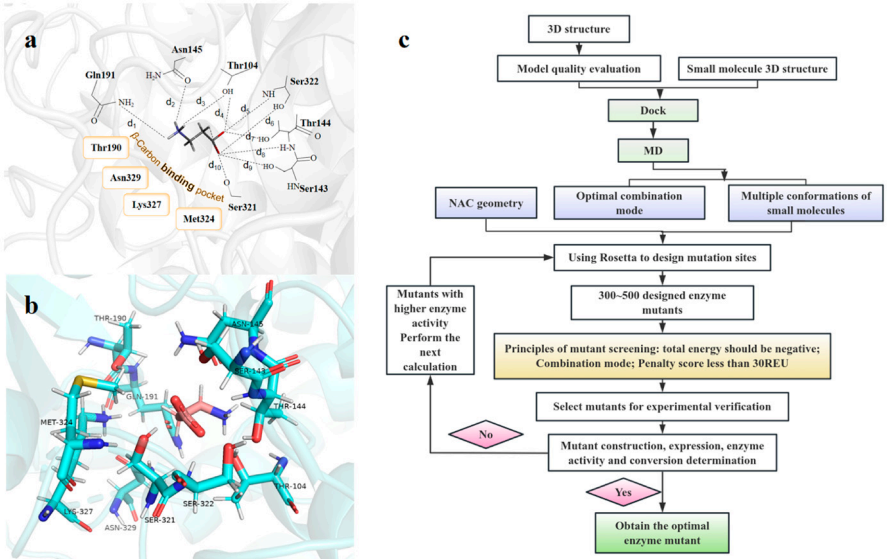


Figure 1. Rational design of aspartase mutants (**a**) Interaction between β-Alanine and AspA, with hydrogen bonds indicated by dotted lines. Residues Thr190, Met324, Lys327, and Asn329 were selected for site-directed mutagenesis, while Asn145 and Glu191 were excluded due to essential catalytic roles. (**b**) Three-dimensional structure of the protein predicted by AlphaFold2 and the docking results of β-Alanine. The AspA amino acid residues are shown in blue, and β-alanine is shown in pink. (**c**) Workflow of Rosetta-based enzyme redesign, including structure prediction, docking, MD simulation, NAC analysis, and multi-step filtering (energy, constraint, hydrogen-bonding, and structural plausibility), leading to 51 selected variants and identification of mutant M1.

The protein sequence of AspA was submitted to AlphaFold2 for structural modeling (Figure S1). After docking β-alanine with AspA (Figure 1b), a 10 ns molecular dynamics simulation was performed, and 10 representative structures were extracted as input for Rosetta calculations. Based on near-attack conformation (NAC) design constraints derived from published QM/MM studies [30]. Rosetta Enzyme Design predicted multiple variants with multi-site mutations to optimize functional interactions between the new substrate and AspA.

Preliminary screening of computationally designed variants was performed using Rosetta Enzyme Design outputs. A total of 881 Rosetta-designed structures were generated from the defined mutation space. These candidates were subjected to a multi-step filtering pipeline. Initially, structures with high constraint penalty scores (all_cst $\geq$ 30 REU) or positive total energy values were excluded. Subsequently, variants lacking preservation of the β-carboxylic acid hydrogen-bond network or exhibiting sterically and energetically unfavorable conformations were removed. In addition, designs containing more than two unsatisfactory hydrogen-bond donors or acceptors were discarded. After computational filtering, the remaining candidates were further evaluated by manual structural inspection to ensure structural plausibility and chemical feasibility. Redundant or highly similar mutation combinations were consolidated to avoid duplication. Finally, 51 representative variants were selected for experimental validation (Table S2), leading to the identification of the optimal mutant M1 (Figure 1c).

2.2. Screening Aspartase Mutants

Using the recombinant plasmid pET28a-AspA as a template, seamless cloning technology was employed to introduce mutation sites. After induction and expression, crude

enzyme extracts were tested to determine their specific enzyme activity and conversion (Table S2). Among the 51 aspartase mutants designed and computationally screened, 38 showed higher activity than the wild type (WT). Among them, M1, M5, M7, and M8 exhibited significantly enhanced activity compared to all other screened mutants. Notably, M1 (T190I–M324I–K327L–N329C) showed a 5.5-fold increase in crude enzyme activity and a 9-fold increase in conversion, compared to the WT enzyme (Table 1). Attempts to introduce high-activity mutations reported in the literature into the WT sequence did not yield satisfactory conversion with acrylic acid.

Table 1. Screened mutants with high activity *.

	AspA Mutant	Specific Enzyme Activity (U/g)	Conversion to β-Alanine (%)	all_cst
WT	-	549.99 ± 17.32	1.49 ± 0.06	-
M1	T190I-M324I-K327L-N329C	3033.33 ± 207.55	13.43 ± 0.63	10.87
M2	T190V-M324I-K327L-N329C	2249.99 ± 217.04	7.24 ± 0.65	11.68
M3	T190I-M324I-K327M-N329C	2000.01 ± 358.68	4.84 ± 0.74	19.32
M4	T190I-K327I-N329C	1999.99 ± 120.26	4.79 ± 0.29	10.16

* all_cst: Total constraint penalty score generated by Rosetta Enzyme Design, representing the degree of violation of geometric and energetic constraints. * Specific activity and conversion were determined experimentally using crude enzyme extracts and quantified by HPLC as described in Section 4.4. Computational parameters (all_cst) were obtained from Rosetta Enzyme Design calculations, where all_cst represents the total constraint penalty score. Data represent mean ± SD (n = 3).

Using M1 as the base, we introduced additional high-activity mutations identified from patents. However, none of the resulting variants outperformed M1 (Table S3) [33]. Notably, although some single-site mutants performed poorly, most multi-site combination mutants showed superior activity. This is likely due to the fact that specificity-enhancing mutations typically occur within the active site, where interactions tend to exhibit non-additive behavior. Therefore, the traditional strategy of sequential single-site mutations followed by combinatorial mutations may no longer be effective. These results underscore the importance of rational combination strategies and demonstrate the effectiveness of Rosetta Enzyme Design.

The mutant M1, with the highest relative activity, and the WT enzyme were purified separately, and their specific activities were compared. After purification and concentration, all proteins were adjusted to an appropriate concentration, and 10 μL of each sample was loaded for protein electrophoresis verification (Figure S1). All mutants and the WT enzyme displayed electrophoretic purity, and their molecular weights were consistent with that of the WT enzyme (~52 kDa).

The optimal reaction temperatures for the WT and mutant enzymes were measured between 25 and 45 °C (Figure 2a). Enzyme activity showed a trend of first increasing and then decreasing with increasing reaction temperature, with the optimal temperature at 37 °C. Within the 25–45 °C range, the specific enzyme activity of the WT enzyme was lower than that of mutant M1. Beyond 40 °C, enzyme activity decreased sharply, likely due to high temperatures disrupting the tertiary structure of the protein.

The residual enzyme activity after 3 h of incubation at 25–45 °C was used to evaluate the enzyme's temperature stability (Figure 2b). The WT enzyme exhibited higher specific activity than the mutant M1, indicating that the mutant's thermal stability was significantly reduced compared to the WT. However, when the temperature exceeded 45 °C, both the WT and mutant enzymes were almost completely inactivated after a 3 h incubation.

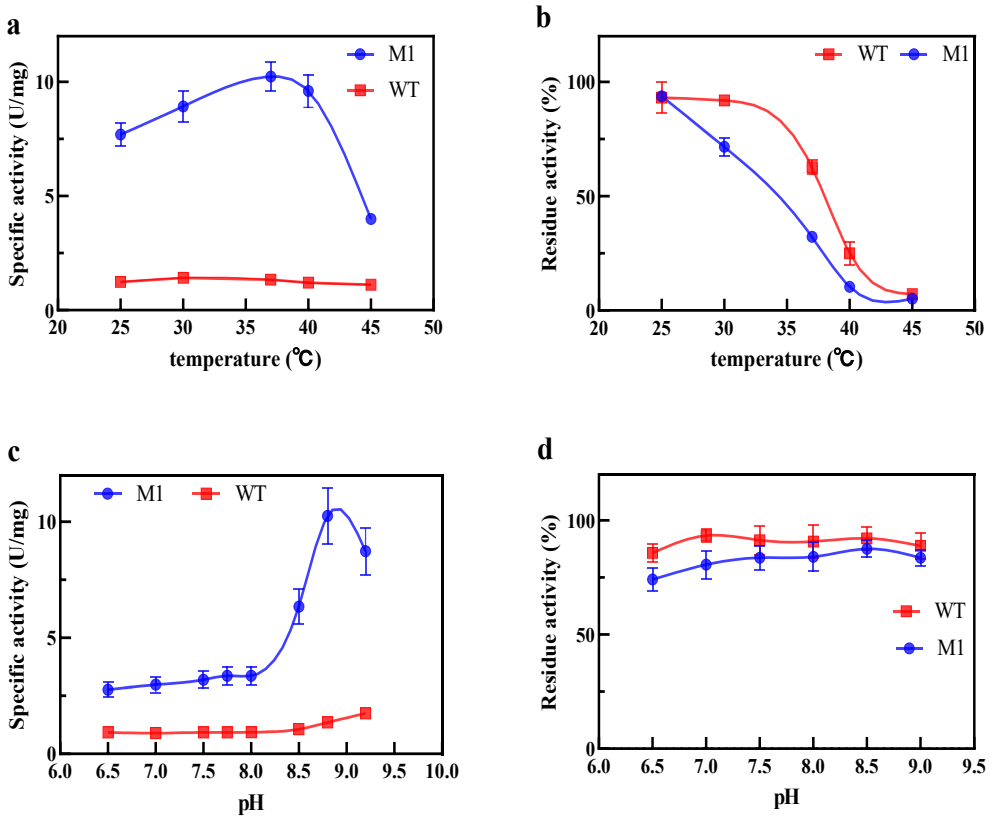


Figure 2. Effects of temperature and pH on the activity of AspA and its mutants. (**a**) Optimum temperature for enzyme activity. (**b**) Thermal stability. (**c**) Optimum pH for enzyme activity. (**d**) pH stability. Enzyme activity was measured using 100 mM acrylic acid and 640 mM ammonia in Tris-HCl buffer (pH 8.8). Reactions were performed at different temperatures (25–45 °C) or pH values for 1 h. β-Alanine formation was quantified by HPLC after derivatization. Data represent mean ± SD (n = 3).

The enzyme activity of the WT and mutant M1 first increased and then decreased with increasing pH (Figure 2c). The optimal pH for the WT enzyme and mutant M1 was 8.8. At pH 6.0–8.0, their activity was relatively low. However, when the pH was between 8.5 and 9.2, the activity of both enzymes increased markedly, suggesting that each enzyme exhibits optimal performance under alkaline conditions.

The stability of mutant M1 was lower than that of the WT enzyme (Figure 2d). When the pH was between 7.0 and 8.5, the mutant retained more activity after 3 h of heating in a 30 °C water bath. However, when the pH was over 8.5 or below 7.0, the residual enzyme activity of both enzymes decreased slightly.

Using different substrate concentrations, the enzyme kinetic parameters of AspA and the mutant M1 were determined, and nonlinear curve fitting was performed using the Michaelis–Menten equation in GraphPad 9.0 software (Table 2). After purification, all mutants exhibited higher specific activities than the WT enzyme, primarily due to increased catalytic constant (k_{cat}), the main factor influencing the biotransformation process. The specific activity and k_{cat} values of M1 were 10.11 U/mg and 262.81 min^{-1}, respectively, while the K_m value of mutant M1 was reduced, indicating an increased affinity for the substrate. Thus, the specificity constant (k_{cat}/K_m) of M1 was 13 times higher than that of the WT enzyme, increasing from 2.02 $mM^{-1}{\cdot}min^{-1}$ to 26.28 $mM^{-1}{\cdot}min^{-1}$, with enzyme activity increasing by 7.3-fold.

Table 2. Kinetic parameters and specific activities of AspA and its mutants *.

Enzyme	K_m (mM)	k_{cat} (min^{-1})	k_{cat}/K_m ($mM^{-1}·min^{-1}$)	Specific Activity ($U·mg^{-1}$)
Wild-type	17.87 ± 3.02	36.10 ± 1.32	2.02 ± 0.13	1.38 ± 0.02
M1	10.00 ± 1.41	262.81 ± 10.26	26.28 ± 2.45	10.11 ± 1.12

* Kinetic parameters (K_m, k_{cat}, and k_{cat}/K_m) were determined by measuring initial reaction rates at varying substrate concentrations and fitted to the Michaelis–Menten equation using GraphPad Prism 9.0 software. Specific activity was determined using purified enzymes under standard assay conditions described in Section 4.4. All values represent the mean of at least three independent experiments ± standard deviation.

2.3. Whole-Cell Catalytic Synthesis of β-Alanine

To improve the catalytic efficiency of M1, whole cells were used as a cost-effective strategy. The catalytic efficiency of M1 was 9.5-fold greater than that of WT AspA, suggesting that M1 represents a beneficial mutation for β-alanine production. To assess the impact of M1 on β-alanine biosynthesis, WT AspA and M1 were used to convert acrylic acid to β-alanine over 12 h at different temperatures and pH values. Between pH 8.0 and 8.8, the conversion of the WT and mutant enzymes increased with increasing pH (Figure 3a), indicating that both enzymes prefer a slightly alkaline environment. This is consistent with the results obtained from the previous pure enzyme pH characterization. At pH 9.0–9.5, the conversion of the mutant began to decrease with rising pH, whereas that of the WT remained relatively unchanged. These results suggest that WT AspA exhibits superior pH stability, whereas the mutant fails to tolerate strongly alkaline conditions.

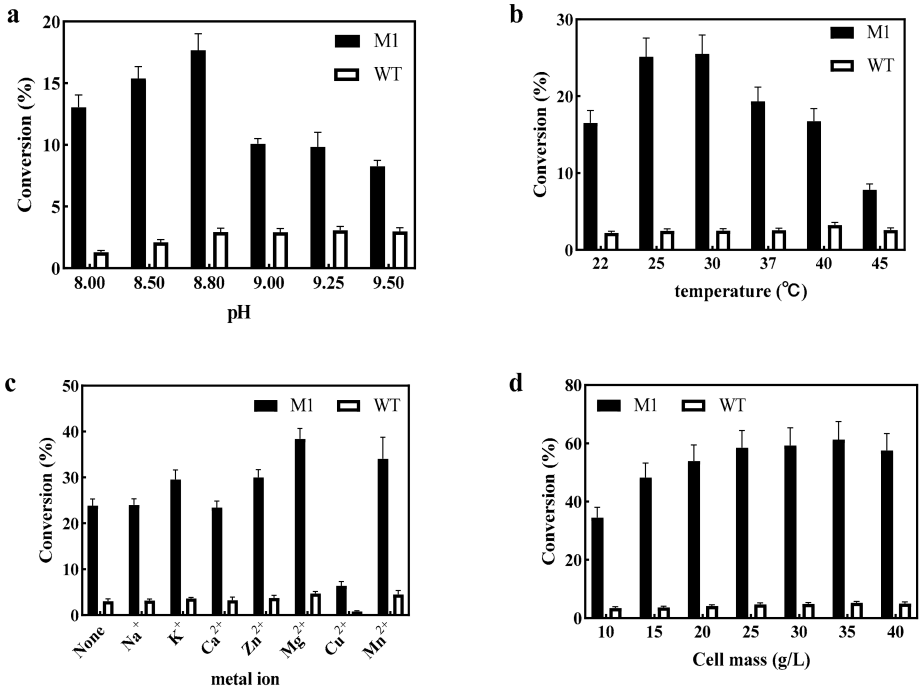


Figure 3. Whole-cell reactions were carried out using recombinant *E. coli* BL21(DE3) expressing AspA or M1. The reaction system contained 100 mM acrylic acid, 640 mM ammonia, and 10 mM $MgSO_4$ in Tris-HCl buffer (pH 8.8). Effects of pH, temperature, metal ions, and cell density were evaluated after 12 h incubation unless otherwise stated. Conversion was quantified by HPLC analysis. Data represent mean ± SD (n = 3). (**a**) Effect of pH on conversion; (**b**) Effect of temperature on conversion; (**c**) Effect of different metal ions on the conversion; (**d**) Effect of cell amount on the conversion.

The conversion for the WT and mutant M1 enzymes increased with increasing temperature (Figure 3b). Notably, the WT enzyme showed a more modest increase in conversion,

suggesting that its activity is less sensitive to temperature changes. When temperatures increased to 37–45 °C, the mutant's conversion dropped significantly, while the WT enzyme performed best at 40 °C. This suggests that the mutant has lower thermal stability than the WT. For optimal enzyme activity, the mutant reacts best at 30 °C.

Metal ions are essential for enzyme-catalyzed reactions, as they modulate enzyme activity and catalytic efficiency. K^+, Zn^{2+}, Mg^{2+}, and Mn^{2+} all promoted enzyme bioconversion, with Mg^{2+} being the most effective activator of aspartase (Figure 3c). In contrast, Cu^{2+} exerted a marked inhibitory effect, reducing M1 conversion to 6.13%. Other metal ions also exhibited either promotional or inhibitory effects, though these effects were comparatively less pronounced. The impact of Mg^{2+} concentration was assessed, with 10 mM Mg^{2+} identified as the optimal concentration (Figure S3). These results demonstrate that metal ions play an important role in regulating AspA catalytic performance, and the effect of Cu^{2+} is further discussed in Section 3.

In biocatalytic reactions, an increase in catalyst quantity typically leads to a higher reaction rate. Thus, it is essential to optimize the catalyst concentration to achieve maximum substrate conversion while reducing catalyst waste and associated costs (Figure S4). The reaction rate increased with cell concentration (Figure 3d). For example, after 12 h of reaction, as the cell concentration increased from 10 g/L to 25 g/L, the substrate conversion gradually increased. However, when the cell concentration increased from 25 g/L to 40 g/L, the reaction reached equilibrium, and the conversion leveled off. Therefore, to optimize biocatalytic efficiency, a final cell concentration of 30 g/L was selected.

The whole-cell catalytic reaction time course reflects the enzymatic reaction kinetics and illustrates the overall behavior of the cells during catalysis. When the cell concentration was set at 30 g/L, the substrate conversion gradually increased during the 12–24 h reaction period (Figure 4). However, extending the reaction time beyond 24 h did not further increase the conversion, which stabilized at 81%. The addition of 60 mM ammonia solution after 18 h of reaction shifted the equilibrium, causing the conversion to reach equilibrium at 48 h and stabilize at 90%, with no subsequent changes. If 60 mM ammonia was added at 24 h, the equilibrium was disturbed, and the conversion reached 89% at 72 h.

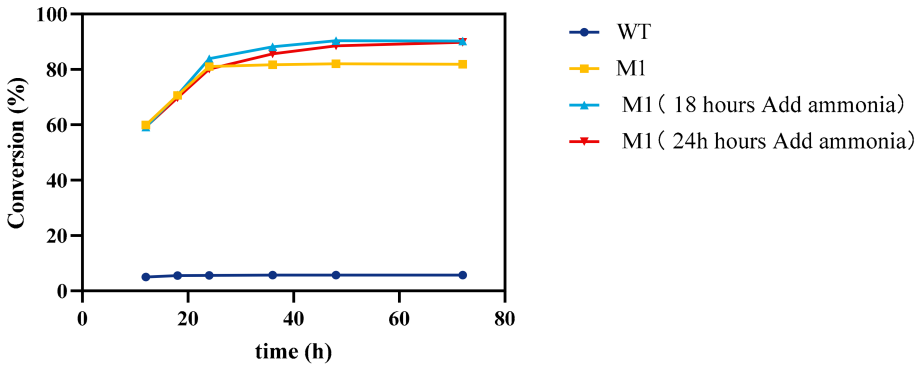


Figure 4. Reaction time profile of whole-cell-catalyzed synthesis of β-alanine. All experiments were conducted under standard conditions described in Materials and Methods Section 4.8, and conversion was quantified by HPLC analysis. Data represent mean ± SD (n = 3). Ammonia feeding was applied at specified time points to modulate reaction equilibrium and improve conversion efficiency.

3. Discussion

Among the tested metal ions, Cu^{2+} exhibited a pronounced inhibitory effect on AspA-mediated β-alanine production. This inhibition may be attributed to the strong coordination ability of Cu^{2+} with amino acid residues such as histidine, cysteine, and acidic residues located in or near the active site. Such interactions can perturb the native hydrogen-bonding network and alter the geometry of the catalytic pocket, leading to reduced catalytic

efficiency. In addition, Cu^{2+} is a redox-active metal ion and may induce local structural perturbations through oxidative modification of sensitive residues, further contributing to enzyme inactivation.

Kinetic simulations using YASARA revealed that AspA functions as a homotetramer, with its active site formed by residues from three separate subunits. The SS loop, containing the characteristic GSSXXPXKXN sequence, is among the most conserved regions within this family of cleaving enzymes and is thought to have a significant role in catalysis [31]. Upon substrate β-alanine binding, the SS loop (residues 317–328) from one subunit may participate in shaping the active-site environment and contribute to substrate accommodation. β-alanine adopts a high-energy conformation and forms a dynamic hydrogen-bond interaction network with residues in the surrounding pocket, which may help stabilize catalytically relevant intermediate states. Crystallographic analysis and mutant experiments have suggested the catalytic role of the SS loop [35]. In its closed-like conformation, Ser321 is situated near the Cβ of β-alanine, which may facilitate proton abstraction during the reaction process. PyMOL visualizations revealed that Gln191, Thr190, Thr104, Ser143, Thr144, Asn146, Lys327, and Ser322 form an extensive hydrogen-bond network with the substrate, helping to stabilize both transition states and intermediates. Using YASARA, we conducted 50-nanosecond molecular dynamics (MD) simulations at 300 K on docking complexes of WT AspA and the M1 mutant with β-alanine. The equilibrated trajectories from the last 10 ns (40–50 ns) were used for subsequent structural analyses. By superimposing the structures of the post-dynamics WT ligand complex and the mutant M1 ligand complex (Figure 5), we suggest that the SS loop in WT tends to remain in a more open-like state. In contrast, the mutant M1 may exhibit a more compact SS-loop conformation upon β-alanine binding.

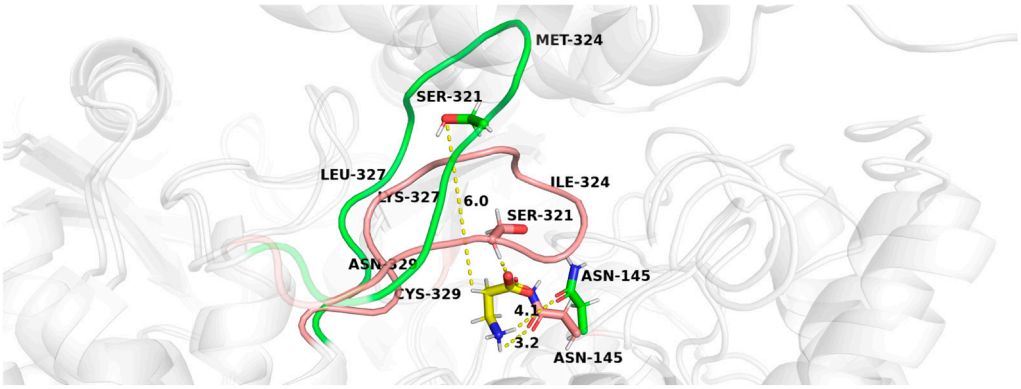


Figure 5. Superposition of WT AspA and mutant M1 structures after 50 ns molecular dynamics simulations in complex with β-alanine. The WT structure is shown in green, the M1 structure is shown in pink, and β-alanine is shown as yellow sticks. The comparison highlights conformational differences in the SS-loop (residues 317–328), with the WT adopting a more open-like conformation and the M1 mutant exhibiting a more compact (closed-like) conformation upon β-alanine binding. WT AspA is shown in green, M1 in pink, and β-alanine in yellow.

Conformational analyses of the mutant and WT enzymes were performed using PyMOL 2.6.0. Structural evaluation revealed that the mutation sites—Met324, Lys327, and Asn329—were all positioned within the S-loop of the AspA tertiary structure. In the M1 mutant, four residues were substituted: Thr190 was mutated to Ile, Met324 to Ile, Lys327 to Leu, and Asn329 to Cys. Notably, three non-hydrophobic amino acids were replaced by hydrophobic residues, whereas Asn329 was exchanged for the smaller side-chain cysteine. These changes may have expanded the substrate-binding pocket and enhanced local hydrophobic interactions. Given that these residues were situated in irregular loop regions,

the mutations likely increased the local conformational flexibility, potentially improving substrate accommodation and catalytic performance. Despite these local changes, the overall hydrogen-bonding network remained relatively stable. Based on these observations, we propose the following hypothesis: the enhanced catalytic activity of the M1 mutant observed in the experiments may be associated with an optimized microenvironment within the active site.

Comparative analysis revealed changes in interaction distances at several mutation sites in the M1 mutant compared to the WT enzyme (Figure 6a,b). Comparative structural analysis revealed that the T190I, M324I, and K327L substitutions reduced the corresponding distances from 4.0 Å to 2.3 Å, 6.5 Å to 2.8 Å, and 3.3 Å to 2.7 Å, respectively, suggesting a more compact local environment. These three hydrophobic mutations likely enhanced local hydrophobic interactions, improving the enzyme's capacity to accommodate methylene groups and increasing its catalytic amination activity.

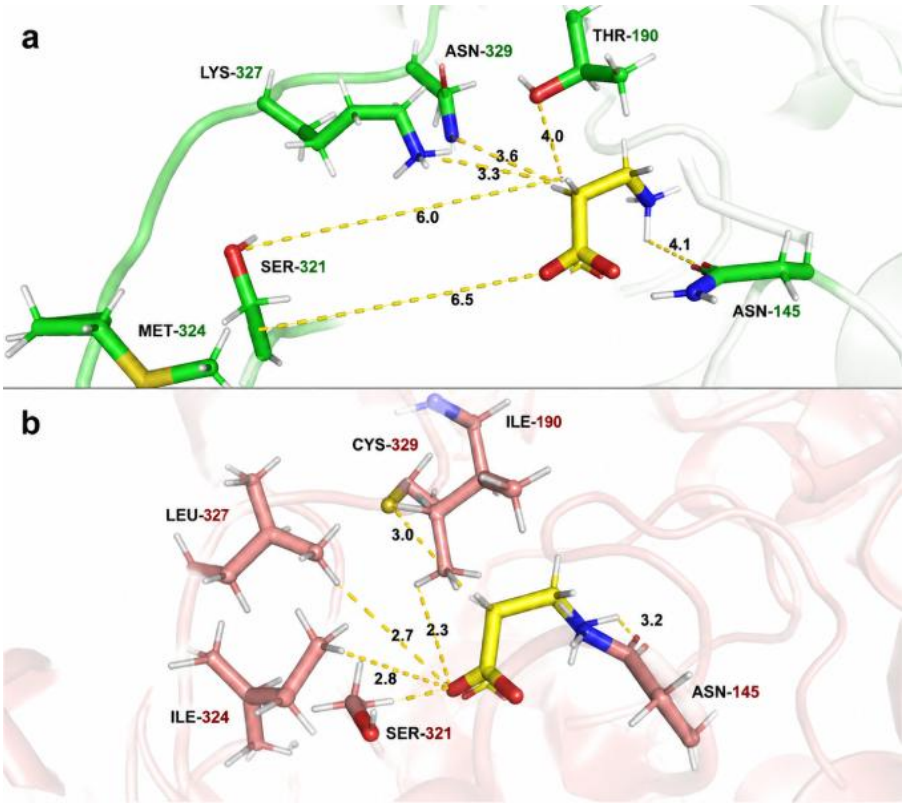


Figure 6. Tertiary structure analysis of wild-type enzyme and mutant enzyme M1. The WT structure is shown in green, the M1 structure is shown in pink, and β-alanine is shown as yellow sticks. (**a**) Local region of wild-type enzyme; (**b**) Local region of mutant enzyme M1. Yellow dashed lines indicate distances between residues and substrate-associated atoms. Corresponding region in M1 mutant showing altered residue interactions and distances. Only representative interactions are shown for clarity.

Additionally, substitution of Asn329 with cysteine decreased the hydrogen bond distance from 3.6 Å to 3.0 Å. The presence of a smaller cysteine side chain may further enlarge the binding pocket, facilitating improved accommodation of small molecules and promoting enzyme–substrate affinity and activity.

Ser321 plays a critical role in the catalytic mechanism of AspA. Structural comparison suggested that the M1 mutations altered the local organization of the catalytic region. Compared with WT AspA, Ser321 in the M1 mutant was positioned in closer proximity to the substrate, which may facilitate substrate positioning and catalytic progression. These

local structural changes could contribute to the enhanced catalytic activity observed for the M1 mutant.

Additionally, Asn145 assists in transferring the amino group during catalysis. Its side chain oxygen bonds with a hydrogen from the substrate's amino group (Figure 6a,b), and this bond shortens from 4.1 Å in the WT enzyme to 3.2 Å in the M1 mutant, suggesting improved positioning for efficient amino group transfer.

Experimentally, the M1 mutant exhibits higher catalytic activity but reduced stability compared with WT AspA (Figure 7). To understand why the M1 mutant is more active but less stable, MD simulations were performed at 300 K over 50 ns for both WT AspA and the M1 mutant bound to β-alanine. The average root mean square fluctuation (RMSF) values were lower for the WT enzyme, indicating it was generally less flexible and more stable (Figure 7). However, in the M1 mutant, residues 301–331 exhibited significantly higher RMSF values, reflecting increased local flexibility. This increased flexibility may facilitate substrate accommodation and product turnover, which could be associated with the improved catalytic efficiency observed in the M1 mutant; we therefore propose this as a mechanistic hypothesis.

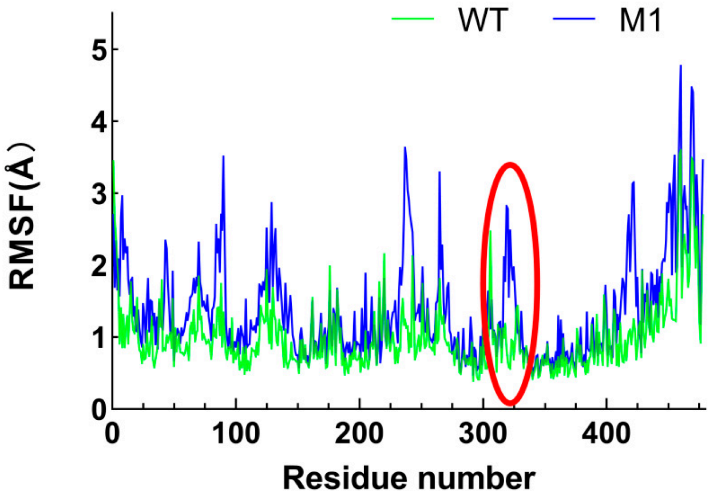


Figure 7. RMSF values of AspA and its mutant M1. RMSF values were calculated from 50 ns molecular dynamics simulations using equilibrated trajectory segments. The red circle indicates the region encompassing residues 301–331, where the M1 mutant exhibits increased flexibility, indicating enhanced local dynamics in the loop region.

Root mean square deviation (RMSD) measures the average deviation between a protein's structure after MD simulation and its initial structure. Examining RMSD fluctuation can help to assess protein stability; smaller fluctuations imply greater structural stability. RMSD profiling revealed that both complexes maintained relatively stable conformations throughout the last 10 ns (40–50 ns) of the 50 ns molecular dynamics simulation (Figure 8).

The RMSD value of the WT enzyme stabilized at approximately 2.0 Å, whereas the M1 mutant's average RMSD stabilized around 3.5 Å. RMSD values for the alpha carbon atoms, main chain, and all heavy atoms also stabilized after brief fluctuations, with ranges within 2 Å. Hence, the overall secondary structure of the WT and M1 mutant enzymes remained stable. These findings indicate that the M1 mutation did not cause notable topological changes relative to WT, supporting the formation of a stable aspartase–β-alanine complex.

Throughout the 50 ns MD simulation, distinct differences in structural fluctuations were noted between the WT and M1 mutant proteins. The mutant proteins exhibited markedly higher RMSD values compared to the WT, indicating increased conformational flexibility and decreased protein stability. Lower RMSD values correlate with greater

rigidity and overall stability. Based on these observations, we hypothesize that the higher structural rigidity of the WT enzyme may be associated with its greater thermal stability compared with the M1 mutant.

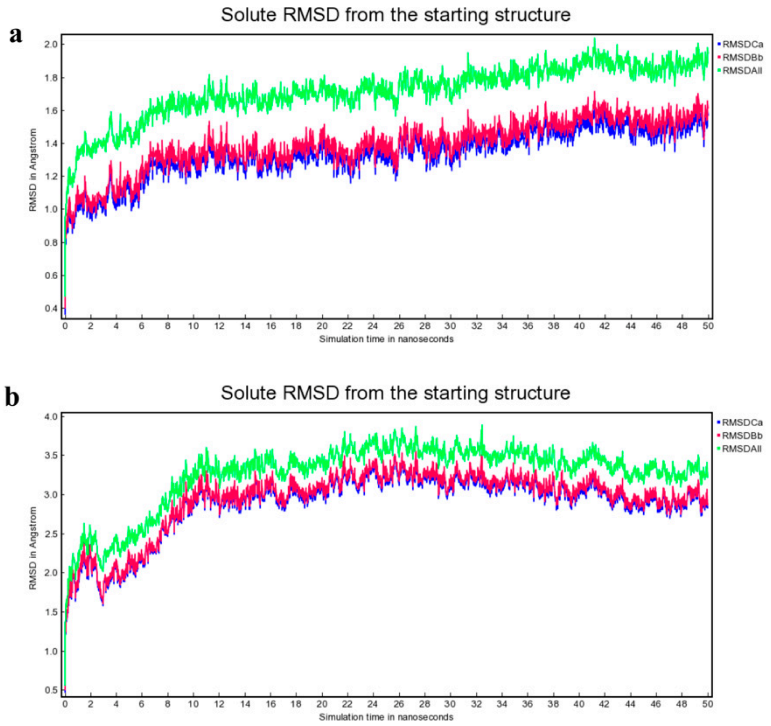


Figure 8. RMSD versus time curve after 50 ns molecular dynamics (MD) simulation. (**a**) MD simulation of AspA and β-alanine complex; (**b**) MD simulation of M1 and β-alanine complex. RMSD values for the alpha carbon atoms (RMSDCα), main chain (RMSDBb), and all heavy atoms (RMSDAll).

From an industrial perspective, the observed trade-off between enhanced catalytic activity and reduced thermal stability in the M1 mutant may have important implications for practical application. Although increased catalytic efficiency is advantageous for improving reaction rates, the decreased structural stability suggested by MD simulations and experimental observations may limit long-term operational performance, particularly under prolonged reaction times or harsh process conditions. To address this limitation, further protein engineering efforts may be required to restore enzyme stability while maintaining the improved catalytic activity of the M1 variant. Potential strategies could include the introduction of stabilizing mutations in surface loops distant from the active site, rational redesign of flexible regions to reduce excessive conformational mobility, or the application of directed evolution approaches to simultaneously optimize stability and activity. Such balance between catalytic efficiency and structural robustness is essential for the development of industrially viable biocatalysts.

The Alejandro Gran–Scheuch team successfully obtained the optimal variant BbAsp-5x through a combination of computational design and genome mining. This variant has a k_{cat} value of 1.3 s^{-1}, a K_m of 250 mM, and a catalytic efficiency (k_{cat}/K_m) of 0.0052 $mM^{-1}{\cdot}s^{-1}$ or 0.312 $mM^{-1}{\cdot}min^{-1}$, which is 83 times lower than the current optimal mutant M1. Furthermore, our analysis indicated that the AspB-A7 variant (T187I-M321I-K324L-N327C), which aligns with the AspA-M1 variant (T190I-M324-K327L-N329C), did not show the greatest improvement in their study. Notably, the AspB-A1 variant (T187I-M321I-K324M-N327C), corresponding to the AspA-M3 variant (T190I-M324I-K327M-N329C), was also not identified as the optimal solution in our investigation [36]. This underscores the complexity

of enzymes of the same class from different sources in terms of structure, function, and areas of application, as well as the importance of experimental validation.

Enhancing the enzymatic activity of the M1 mutant leads to a certain degree of reduced stability. In future studies, various rational design methods can be applied to improve thermal stability, focusing on mutations outside the active site to enhance enzyme stability without compromising catalytic activity. This strategy can provide valuable guidance for subsequent engineering of aspartase enzymes. Furthermore, integrating additional rational design approaches with artificial intelligence technologies holds promise for further optimizing enzyme activity.

Protein engineering substantially improved the intrinsic catalytic performance of the enzyme, increasing the conversion of acrylic acid to β-alanine from 1% (WT) to 13% (M1 mutant). Building on this improvement, whole-cell biocatalytic performance was further enhanced to 90% conversion through systematic optimization of reaction conditions, including pH, temperature, Mg^{2+} concentration, cell density, substrate ratio, and ammonia feeding strategy, highlighting the combined contribution of enzyme engineering and process optimization.

From an industrial perspective, although the engineered whole-cell system achieved a high conversion (~90%) after process optimization, several practical limitations should be considered. First, the substrate concentration (100 mM acrylic acid) remains relatively low compared with typical industrial biocatalytic processes, which may limit overall space–time yield. Second, the reaction requires a relatively high whole-cell loading (30 g/L) and an extended reaction time (up to 48 h), which could increase production costs and reduce process efficiency. In addition, the final product concentration and productivity are still constrained by potential mass transfer limitations and substrate/product inhibition effects under high-density whole-cell systems. The stability of the biocatalyst during prolonged operation may also represent a bottleneck for continuous or large-scale applications. Furthermore, scale-up of the current system may face challenges related to oxygen transfer, mixing efficiency, and maintenance of optimal reaction conditions in industrial bioreactors. Therefore, while the present system demonstrates promising catalytic performance at laboratory scale, further process intensification strategies—such as increasing substrate loading, improving enzyme stability, and optimizing reactor design—will be necessary to enhance its industrial applicability.

4. Materials and Methods

4.1. Chemicals, Plasmids, and Strains

All chemicals were of analytical grade. PrimeSTAR® Max DNA polymerase and Dpn I were purchased from Takara Biotechnology (Dalian, China). The Universal DNA Purification Kit, TIANpure Mini Plasmid Kit, and DNA marker (500–7000 bp) were purchased from Tiangen Biotech Co., Ltd. (Beijing, China). A regular range protein marker (15–130 KDa) was obtained from Sangon Biotech Co., Ltd. (Shanghai, China). *Escherichia coli* BL21(DE3) was used as a host for heterologous expression. The recombinant plasmid pET28a-AspA was constructed in our previous work [13].

4.2. Aspartase Computational Redesign

The AspA prediction model was constructed using AlphaFold2 (version 2.3.2, DeepMind, London, UK, 2023) on the Beikun Cloud high-performance computing platform (Shenzhen, China) [30]. The model's quality was validated using PROCHECK (https://saves.mbi.ucla.edu/, accessed 10 December 2023) [31,32]. The docked products were introduced into the AspA-predicted model using the dock_run script in YASARA Struc-

ture (version 22.5.22, YASARA Biosciences GmbH, Vienna, Austria, 2022) [33] to dock the product β-alanine to the AspA-predicted model.

A 10 ns kinetic simulation was conducted using the md_run script in YASARA. First, the complex was immersed in a water model, and counterions were added to neutralize the system's charge. Periodicity was applied, and the protein and small molecules were optimized. The system was then minimized to eliminate unreasonable side-chain structures in the amino acids. The system temperature was gradually increased from 0 K to 310 K, followed by a 10 ns kinetic simulation, with ten structures extracted as input for Rosetta calculations.

Computational design was performed using Rosetta enzyme design [35], inputting the complexes obtained from kinetic simulations and using the following command line options: -enzdes-cst_predock-cst_design-detect_design_interface-cut1 0.0-cut2 0.0-cut3 8.0-cut4 10.0-cst_min-chi_min-bb_min-packing::use_input_sc-packing::soft_rep_design -extrachi_cutoff 1-design_min_cycles3-ex1:level 4-ex2:level 4-ex1aro:level 4-ex2aro:level 4.

The Rosetta Enzyme Design application applies forces between ligands and enzymes' key catalytic groups to position them in the optimal catalytic conformation. The near-attack conformation of the complex was determined based on published QM/MM quantum-chemical calculations [24] and the crystal structure of AspB bound to the substrate (PDB: 3R6V). Rosetta Enzyme Design uses the Monte Carlo algorithm to select mutations and structural changes that reduce the overall energy, thereby generating the designed 3D structure. Predefined constraints that penalize non-catalytic conformations of catalytic residues were applied in Rosetta Enzyme Design calculations (Table S1). The constraints are established such that any deviation of the catalytic residue from its catalytic conformation incurs a penalty. Catalytic constraints are formally represented by specified distances, angles, and dihedral relationships between the catalytic residue and the substrate.

Designs were selected for experimental characterization based on the following criteria: (1) total penalty energy from the constraints was $\leq$30 REU, (2) the original carboxylic acid hydrogen bond network remained intact, (3) mutations did not produce unreasonable structures, and (4) total energy was negative.

The mutant was generated from the pET28a-AspA plasmid using seamless cloning technology (Table S1). The PCR mix (50 μL) comprised 2× PrimeSTAR®Max DNA polymerase (25 μL), forward and reverse primers (1 μL, 10 μM), plasmid DNA (pET28a-AspA, 1 μL), and sterilized water (22 μL). The reaction program was as follows: 95 °C for 10 min, 24 cycles at 98 °C for 10 s, 56 °C for 15 s, 72 °C for 75 s; final extension at 72 °C for 5 min. PCR products were digested with Dpn I at 37 °C for 4 h, then transformed into *E. coli* BL21 (DE3) and cultured overnight on Luria–Bertani (LB) plates. Transformant sequences were verified using DNA sequencing. Primers were synthesized by BGI (Beijing, China) and are listed in Table S4.

4.3. Enzyme Expression and Purification

4.3.1. Culture Conditions for Recombinant Bacteria and Crude Enzyme Preparation

The bacterial suspension was transferred from the glycerol tube to LB agar with 50 μg/mL kanamycin using an inoculation loop, then streaked onto a plate. The plate was incubated at 37 °C for 12–16 h. A single colony was selected and inoculated into LB liquid medium containing 50 μg/mL kanamycin. The culture was incubated at 37 °C with agitation at 200 rpm for 12 h until the OD_{600} reached approximately 0.3 to produce the seed culture.

The fermentation medium was prepared by introducing 2% of the seed culture into 2YT medium supplemented with 50 μg/mL kanamycin. The culture was incubated at 37 °C with shaking at 200 rpm for 2 h, until the OD_{600} reached approximately 0.3. IPTG

was then added to achieve a final concentration of 0.2 mM, and protein expression was induced at 24 °C with continuous shaking at 200 rpm for 20 h. Subsequently, the cells were harvested by centrifugation at 8000 rpm for 15 min at 4 °C. The pellet was washed twice with physiological saline and resuspended in 200 mM Tris-HCl (pH 8.5) to 10 g_{dcw}/L. The cells were disrupted using a high-pressure cell disruptor at 4 °C and 1296 bar, with the process repeated twice. Following disruption, the mixture was centrifuged at 4 °C and 5000 rpm for 30 min. The resulting supernatant was considered the crude enzyme solution.

4.3.2. Protein Purification

Lysis buffer (50 mM NaH_2PO_4, 300 mM NaCl, 10 mM imidazole, pH 8.5) was added to the collected bacterial cells and resuspended to a concentration of 10 g_{dcw}/L. The suspension was placed in a beaker containing ice water. A 10 mL aliquot of the bacterial suspension was disrupted using an ultrasonic disruptor under the same conditions described above. After centrifugation at 4 °C and 12,000 rpm for 30 min. The proteins in the supernatant were purified using a Ni-NTA Beads6FF gravity column (Tian Di Ren He Biotechnology Co., Ltd., Changzhou, China) according to the manufacturer's instructions. The purified protein was concentrated using a Millipore ultrafiltration centrifuge tube (10 kDa) and exchanged three or more times with 200 mM Tris-HCl buffer (pH 8.8) at 4 °C and 5000 rpm for 50 min to completely remove imidazole. All purified enzymes were diluted to 0.6 mg/mL for sodium dodecyl sulfate-polyacrylamide gel electrophoresis analysis to assess purification efficiency. Protein concentration was determined using the Bradford assay, with bovine serum albumin as the standard (Takara).

4.3.3. Enzyme Activity Assay Method

The reaction system comprised 200 mM Tris-HCl buffer (pH 8.8), 100 mM acrylic acid, 640 mM ammonia, 10 mM $MgSO_4 \cdot 7H_2O$, and an appropriately diluted enzyme solution, incubated at 37 °C for 1 h. After derivatization, the sample was filtered through a 0.45 μm organic filter membrane, and the β-alanine concentration was analyzed using HPLC (LC-20AT, Shimadzu, Kyoto, Japan). Enzyme activity was defined as the amount of enzyme required to produce 1 μmol of β-alanine per min at 37 °C and pH 8.8, corresponding to one enzyme activity unit (U).

4.4. Experimental Method for Screening Aspartase Mutants

The reaction system comprised 200 mM Tris-HCl buffer (pH 8.5), 400 mM acrylic acid (pH adjusted with 25% ammonia solution), 10 mM $MgSO_4 \cdot 7H_2O$, and an appropriately diluted enzyme solution, and was incubated at 37 °C for 12 h. After derivatization, the sample was filtered through a 0.45 μm organic filter membrane, and the β-alanine concentration was analyzed by HPLC using a calibration curve.

4.5. HPLC Analysis Methods

For the PITC derivatization reaction, 400 μL of the reaction solution was combined with 200 μL of 1 M triethylamine-acetonitrile and 200 μL of 0.1 M PITC-acetonitrile, and the mixture was mixed thoroughly. The solution was derivatized in the dark for 1 h before adding 500 μL of hexane to terminate the reaction. A vortex mixer was employed to shake for 1 min to fully extract any excess organic solvent, followed by centrifugation at 12,000 rpm for 2 min. The lower layer of the extracted solution was filtered using a 0.45-μm water-based filter membrane before conducting liquid chromatography analysis. The HPLC detection method was then employed (Table S5).

4.6. Enzymatic Characterization

4.6.1. Optimizing Reaction Temperature and Temperature Stability

To determine the optimal reaction temperature, 0.05 mg (final concentration 0.05 mg/mL) of pure enzyme was combined with substrate at a final concentration of 100 mM (pH 8.8). Enzyme activity was measured at 25 °C, 30 °C, 37 °C, 40 °C, and 45 °C using the above enzyme activity assay method.

To evaluate temperature stability, 0.05 mg of pure enzyme was incubated at 25 °C, 30 °C, 37 °C, 40 °C, and 45 °C for 3 h. The samples were then cooled on crushed ice for 5 min. Residual enzyme activity was measured at 37 °C and pH 8.8 using the above enzyme activity assay method, with initial enzyme activity at each temperature set as 100%.

4.6.2. Optimizing Reaction pH and pH Stability

To determine the optimal reaction pH, 0.05 mg of pure enzyme (final concentration: 0.05 mg/mL) was combined with 100 mM substrate (pH 8.8) and reacted in buffers of varying pH, using the above enzyme activity assay method. Phosphate buffers at pH 6.5, 7.0, 7.5, and 7.75, and Tris-HCl buffers at pH 8.0, 8.5, 8.8, and 9.2 were used for the reactions.

For pH stability analysis, 0.05 mg of pure enzyme was mixed with the activity measurement system and buffers of different pH values. The mixtures were incubated at 30 °C for 3 h, after which residual enzyme activity was measured as enzyme activity assay method. The initial enzyme activity at each pH was set as 100%. The same buffers as described above were used for these experiments.

4.7. Determination of Kinetic Parameters of AspA and Its Mutants

In a 1 mL reaction system, 500 μL of pure enzyme (0.1 mg) was mixed with 500 μL of substrate at concentrations of 2, 4, 8, 12, 20, 60, 100, and 200 mM, resulting in final substrate concentrations of 2, 4, 8, 12, 20, 60, 100, and 200 mM. After incubation at 37 °C for an appropriate time, the reaction was terminated, and the amount of product was measured. The initial reaction rate was calculated by dividing the amount of β-alanine produced by the reaction time. Substrate concentration values were plotted on the *x*-axis and reaction rates on the *y*-axis. Nonlinear fitting was performed using GraphPad Prism (Version 8.0, GraphPad Software Inc., San Diego, CA, USA, 1995) to determine the apparent kinetic constants (K_m and Vmax) and the catalytic constant (k_{cat}).

4.8. Experimental Method for Whole-Cell Catalytic Synthesis of β-Alanine

To optimize reaction pH, 0.2 M Tris-HCl solutions at pH 8.0, 8.5, 8.8, and 9.0, and 0.2 M Gly-NaOH solutions at pH 9.25 and 9.5 were prepared. For the stock solution, 2.88 mL of acrylic acid (final concentration 400 mM) was added to 10 mL of $MgSO_4 \cdot 7H_2O$ (final concentration 10 mM). The pH was adjusted to 8.5 with 25% ammonia solution, and the solution was diluted to 100 mL with 0.2 M Tris-HCl buffer at pH 8.5 before being thoroughly mixed. For the reaction setup, 500 μL of cells and 500 μL of stock solution were combined in a 1 mL reaction system, mixed thoroughly, preheated at 37 °C for 2 min, and then reacted at 37 °C and 1000 rpm for 12 h. After derivatization, samples were filtered through a 0.45 μm organic filter membrane, and the β-alanine and acrylic acid contents in the liquid phase were measured.

The reaction temperature was optimized using a reaction system containing 1 mL of 400 mM substrate, 10 g/L cells, and 0.2 M Tris-HCl buffer (pH 8.8). Catalytic reactions were conducted at 22 °C, 25 °C, 30 °C, 37 °C, 40 °C, and 45 °C. Samples were collected after 12 h of reaction to measure the conversion.

The effects of metal ions were assessed in enzyme reaction systems to which 10 mM metal salt solutions—NaCl, KCl, $CaCl_2$, $ZnCl_2$, $MgSO_4 \cdot 7H_2O$, $CuCl_2 \cdot 2H_2O$, and

$MnCl_2 \cdot 4H_2O$—were added, and enzyme activity was recorded. The results were compared with those obtained with $MgSO_4 \cdot 7H_2O$ to assess the extent to which these metal ions activated the enzyme. The reaction system contained 1 mL of solution with a cell concentration of 10 g/L. A stock solution was prepared using a ratio of 0.1 M acetic acid to 0.64 M ammonia water. The buffer solution was 0.2 M Tris-HCl (pH = 8.8). After reacting at 30 °C and 1000 rpm for 12 h, samples were collected to measure the conversion.

To assess the impact of cell density, the reaction system had a total volume of 1 mL, with a substrate concentration of 100 mM (prepared at a ratio of 0.1 M acrylic acid to 0.64 M ammonia water), and a buffer solution of 0.2 M Tris-HCl (pH = 8.8). The cell amounts were varied at 10, 15, 20, 25, 30, 35, 40, and 50 g/L. Samples were collected after 1 h of reaction at 30 °C and 1000 rpm to measure the conversion.

The reaction time course was evaluated in a reaction system containing 1 mL total volume, 100 mM substrate (prepared at a 0.1 M acrylic acid:0.64 M ammonia water ratio), 30 g/L cells, and 0.2 M Tris-HCl buffer (pH 8.8). Samples were collected and analyzed for conversion at 30 °C and 1000 rpm after 12, 18, 24, 36, 48, and 72 h of reaction.

After 24 h of reaction, the system approached equilibrium. To drive the equilibrium toward β-alanine production, ammonia was added midway through the process to assess optimal replenishment timing. The reaction system had a total volume of 1 mL, with a substrate concentration of 100 mM (prepared at a 0.1 M acrylic acid:0.64 M ammonia water ratio), a cell density of 30 g/L, and 0.2 M Tris-HCl buffer (pH 8.8). Reactions were conducted at 30 °C with agitation at 1000 rpm, and aqueous ammonia was supplemented at 18 h and 24 h. Samples were collected at 12, 18, 24, 36, 48, and 72 h for analysis of conversion.

5. Conclusions

In this study, AspA from *E. coli* was selected for rational design-based enzyme molecular modification to improve its biocatalytic efficiency in β-alanine synthesis. Computational analysis using Rosetta was performed on AspA complexes with small molecules and descriptive data, yielding 51 mutant candidates. The mutations were constructed, expressed, and evaluated for catalytic function in crude enzyme preparations, ultimately identifying the optimal mutant, M1 (T190I-M324I-K327L-N329C). Although the optimal pH and temperature profiles of both WT and mutant M1 were comparable, M1 demonstrated reduced stability relative to the WT protein.

Kinetic parameter evaluation revealed a notable increase in the catalytic constant (k_{cat}) for the mutant, underscoring its impact on biotransformation performance. Mutant M1 exhibited specific activity and k_{cat} values of 10.11 U/mg and 262.81 min^{-1}, respectively, whereas the K_m value decreased, indicating enhanced substrate affinity. Therefore, the specificity constant (k_{cat}/K_m) of M1 was 13 times higher than that of the WT enzyme, increasing from 2.02 $mM^{-1} \cdot min^{-1}$ to 26.28 $mM^{-1} \cdot min^{-1}$, whereas the enzymatic activity increased by 7.3-fold.

Optimization of whole-cell biocatalytic conditions enabled the use of 30 g/L of M1 cells to catalyze the reaction between 100 mM acrylic acid and 640 mM aqueous ammonia at 30 °C and pH 8.8 for 48 h. An additional 60 mM of aqueous ammonia was added at 18 h, resulting in a conversion of 90%. This computational redesign strategy offers valuable insights as a reference framework for the rational engineering of other enzymes.

Supplementary Materials: The following supporting information can be downloaded at: https://www.mdpi.com/article/10.3390/catal16070647/s1, Figure S1: 3D structure of AspA modeling; Figure S2: SDS-PAGE of wild-type and M1mutant of AspA; Figure S3: Effect of magnesium ion concentration on the conversion of β-alanine; Figure S4: Effect of the ammonia water-to-acrylic acid molar ratio on the conversion of β-alanine; Table S1: Design constraints for maintaining the catalytic state of AspA; Table S2: Measurement results of AspA mutants constructed in this work; Table S3:

Measurement results of previously reported AspA mutants; Table S4: Primers for site-directed mutagenesis; Table S5: HPLC analytical method of β-alanine. Additional references related to previously reported AspA mutants and patents used for comparison in the computational screening are cited in the Supplementary Materials and are included in the main reference list [37–43].

Author Contributions: Conceptualization, Y.X.; methodology, B.-D.M. and Y.X.; software, L.-X.L.; validation, L.-X.L.; formal analysis, L.-X.L.; investigation, L.-X.L.; resources, Y.X.; data curation, L.-X.L.; writing—original draft preparation, L.-X.L.; writing—review and editing, B.-D.M. and Y.X.; visualization, L.-X.L.; supervision, Y.X.; project administration, Y.X.; funding acquisition, Y.X. and B.-D.M. All authors have read and agreed to the published version of the manuscript.

Funding: This work was supported by the National Natural Science Foundation of China (No. 32101230), Shanghai Committee of Science and Technology (No. 13430503400), the Project of Leading Talents in Shandong Taishan Industry (No. LJNY202019) and the Recruitment Program of Foreign Faculty Members of Shanghai Institute of Technology (No. 1021GK210004008).

Data Availability Statement: The original contributions presented in this study are included in the article/Supplementary Material. Further inquiries can be directed to the corresponding author.

Conflicts of Interest: The authors declare no conflicts of interest.

Abbreviations

The following abbreviations are used in this manuscript:

AspA	Aspartase from *Escherichia coli*
NAC	Near-attack conformation
WT	Wild type
MD	Molecular dynamics
RMSF	Root mean square fluctuation
RMSD	Root mean square deviation
LB	Luria–Bertani
HPLC	High-performance liquid chromatography

References

1. Ko, Y.-S.; Kim, J.W.; Chae, T.U.; Song, C.W.; Lee, S.Y. A novel biosynthetic pathway for the production of acrylic acid through β-alanine route in *Escherichia coli*. *ACS Synth. Biol.* **2020**, *9*, 1150–1159. [CrossRef] [PubMed]
2. Chen, S.; Zhang, M.; Wu, X.; Bai, F.; Gao, L.; Shen, Y.; Dou, S.; Cai, P.; Zhou, Y.J. Promoter engineering for enhanced 3-hydroxypropionic acid production in *Pichia pastoris*. *Synth. Syst. Biotechnol.* **2025**, *10*, 916–924. [CrossRef] [PubMed]
3. Lacmata, S.T.; Kuiate, J.R.; Ding, Y.; Xian, M.; Liu, H.; Boudjeko, T.; Feng, X.; Zhao, G. Enhanced poly(3-hydroxypropionate) production via β-alanine pathway in recombinant *Escherichia coli*. *PLoS ONE* **2017**, *12*, e0173150. [CrossRef] [PubMed]
4. Tadi, S.R.R.; Nehru, G.; Sivaprakasam, S. Metabolic engineering of Bacillus megaterium for the production of β-alanine. *Biotechnol. Bioprocess. Eng.* **2022**, *27*, 909–920. [CrossRef]
5. Kim, M.; Ko, Y.J.; Jeong, D.W.; Jeong, W.Y.; Han, S.O. Ecofriendly synthesis of L-carnosine in metabolically engineered Corynebacterium glutamicum by reinforcing precursor accumulation. *ACS Synth. Biol.* **2021**, *10*, 1553–1562. [CrossRef] [PubMed]
6. Chen, M.L.; Qi, Y.; Xiao, Y.M.; Hua, C.; Li, J.Y.; Liang, A.P. Biocatalytic synthesis of β-alanine from fumaric acid by a two-enzyme system. *Bull. Ferment. Sci. Technol.* **2018**, *47*, 231–235. [CrossRef]
7. Hooshmand, S.; Halabchi, F.; Hashempour, A.; Rajabian Tabesh, M.; Alizadeh, Z. Improving physical activity tolerance in sedentary overweight women under beta-alanine supplementation. *Sci. Sports* **2019**, *34*, e217–e223. [CrossRef]
8. Chakauya, E.; Coxon, K.M.; Whitney, H.M.; Ashurst, J.L.; Abell, C.; Smith, A.G. Pantothenate biosynthesis in higher plants: Advances and challenges. *Physiol. Plant* **2006**, *126*, 319–329. [CrossRef]
9. Steunenberg, P.; Könst, P.M.; Scott, E.L.; Franssen, M.C.R.; Zuilhof, H.; Sanders, J.P.M. Polymerisation of β-alanine through catalytic ester–amide exchange. *Eur. Polym. J.* **2013**, *49*, 1773–1781. [CrossRef]
10. Wang, L.; Mao, Y.; Wang, Z.; Ma, H.; Chen, T. Advances in biotechnological production of β-alanine. *World J. Microbiol. Biotechnol.* **2021**, *37*, 79. [CrossRef] [PubMed]

11. Li, B.; Zhang, B.; Wang, P.; Cai, X.; Chen, Y.Y.; Yang, Y.F.; Liu, Z.Q.; Zheng, Y.G. Rerouting fluxes of the central carbon metabolism and relieving mechanism-based inactivation of l-aspartate-α-decarboxylase for fermentative production of β-alanine in *Escherichia coli*. *ACS Synth. Biol.* **2022**, *11*, 1908–1918. [CrossRef] [PubMed]
12. Wang, P.; Zhou, H.-Y.; Li, B.; Ding, W.-Q.; Liu, Z.-Q.; Zheng, Y.-G. Multiplex modification of *Escherichia coli* for enhanced β-alanine biosynthesis through metabolic engineering. *Bioresour. Technol.* **2021**, *342*, 126050. [CrossRef] [PubMed]
13. Wu, J.; Ma, B.-D.; Xu, Y. One-pot synthesis of β-alanine from maleic acid via three-enzyme cascade biotransformation. *Catalysts* **2023**, *13*, 267. [CrossRef]
14. Huang, L.; Wang, W.; Wang, K.; Li, Y.; Zhou, J.; Pang, A.; Zhang, B.; Liu, Z.; Zheng, Y. Protein rational design and modification of erythrose reductase for the improvement of erythritol production in Yarrowia lipolytica. *Bioprocess. Biosyst. Eng.* **2024**, *47*, 1659–1668. [CrossRef] [PubMed]
15. Conley, E.; Wadler, C.S.; Bell, B.A.; Lucier, I.; Haynie, C.; Eldred, S.; Nguyen, V.; Bugni, T.S.; Thomas, M.G. Directed evolution of an adenylation domain alters substrate specificity and generates a new catechol siderophore in *Escherichia coli*. *Biochemistry* **2024**, *63*, 3126–3135. [CrossRef] [PubMed]
16. Wang, C.X.; Hu, B.; Yang, Y.; Wang, Y.; Qin, J.; Wen, X.; Li, Y.; Li, H.; Wang, Y.; Wang, J.; et al. Structural simulation and selective inhibitor discovery study for histone demethylases KDM4E/6B from a computational perspective. *Comput. Biol. Chem.* **2024**, *110*, 108072. [CrossRef] [PubMed]
17. Koo, N.K.; Han, S.M.; Kim, S.B.; Baek, S.H.; Park, H.J. Establishment of high-throughput screening protocol based on isomerase using *Geobacillus* sp. L-rhamnose isomerase. *J. Microbiol. Biotechnol.* **2025**, *35*, e2507026. [CrossRef] [PubMed]
18. Jochens, H.; Bornscheuer, U.T. Natural diversity to guide focused directed evolution. *ChemBioChem* **2010**, *11*, 1861–1866. [CrossRef] [PubMed]
19. Parvez, A.; Ravikumar, Y.; Bisht, R.; Yun, J.; Wang, Y.; Chandrika, S.P.; Zabed, H.M.; Qi, X. Functional and structural roles of the dimer interface in the activity and stability of Clostridium butyricum 1,3-propanediol oxidoreductase. *ACS Synth. Biol.* **2022**, *11*, 1261–1271. [CrossRef] [PubMed]
20. Lutz, S. Beyond directed evolution—Semi-rational protein engineering and design. *Curr. Opin. Biotechnol.* **2010**, *21*, 734–743. [CrossRef] [PubMed]
21. Moroz, Y.S.; Dunston, T.T.; Makhlynets, O.V.; Moroz, O.V.; Wu, Y.; Yoon, J.H.; Olsen, A.B.; McLaughlin, J.M.; Mack, K.L.; Gosavi, P.M.; et al. New tricks for old proteins: Single mutations in a nonenzymatic protein give rise to various enzymatic activities. *J. Am. Chem. Soc.* **2015**, *137*, 14905–14911. [CrossRef] [PubMed]
22. Huang, P.S.; Boyken, S.E.; Baker, D. The coming of age of de novo protein design. *Nature* **2016**, *537*, 320–327. [CrossRef] [PubMed]
23. Wu, L.; Qin, L.; Nie, Y.; Xu, Y.; Zhao, Y.-L. Computer-aided understanding and engineering of enzymatic selectivity. *Biotechnol. Adv.* **2022**, *54*, 107793. [CrossRef] [PubMed]
24. Richter, F.; Leaver-Fay, A.; Khare, S.D.; Bjelic, S.; Baker, D. De novo enzyme design using Rosetta3. *PLoS ONE* **2011**, *6*, e19230. [CrossRef] [PubMed]
25. Röthlisberger, D.; Khersonsky, O.; Wollacott, A.M.; Jiang, L.; DeChancie, J.; Betker, J.; Gallaher, J.L.; Althoff, E.A.; Zanghellini, A.; Dym, O.; et al. Kemp elimination catalysts by computational enzyme design. *Nature* **2008**, *453*, 190–195. [CrossRef] [PubMed]
26. Jiang, L.; Althoff, E.A.; Clemente, F.R.; Doyle, L.; Röthlisberger, D.; Zanghellini, A.; Gallaher, J.L.; Betker, J.L.; Tanaka, F.; Barbas, C.F.; et al. De novo computational design of retro-aldol enzymes. *Science* **2008**, *319*, 1387–1391. [CrossRef] [PubMed]
27. Siegel, J.B.; Zanghellini, A.; Lovick, H.M.; Kiss, G.; Lambert, A.R.; St Clair, J.L.; Gallaher, J.L.; Hilvert, D.; Gelb, M.H.; Stoddard, B.L.; et al. Computational design of an enzyme catalyst for a stereoselective bimolecular Diels-Alder reaction. *Science* **2010**, *329*, 309–313. [CrossRef] [PubMed]
28. Khare, S.D.; Kipnis, Y.; Greisen, P.; Takeuchi, R.; Ashani, Y.; Goldsmith, M.; Song, Y.; Gallaher, J.L.; Silman, I.; Leader, H.; et al. Computational redesign of a mononuclear zinc metalloenzyme for organophosphate hydrolysis. *Nat. Chem. Biol.* **2012**, *8*, 294–300. [CrossRef] [PubMed]
29. Asano, Y.; Kira, I.; Yokozeki, K. Alteration of substrate specificity of aspartase by directed evolution. *Biomol. Eng.* **2005**, *22*, 95–101. [CrossRef] [PubMed]
30. Zhang, J.; Liu, Y. A QM/MM study of the catalytic mechanism of aspartate ammonia lyase. *J. Mol. Graph. Model.* **2014**, *51*, 113–119. [CrossRef] [PubMed]
31. Puthan Veetil, V.P.; Fibriansah, G.; Raj, H.; Thunnissen, A.M.W.H.; Poelarends, G.J. Aspartase/fumarase superfamily: A common catalytic strategy involving general base-catalyzed formation of a highly stabilized aci-carboxylate intermediate. *Biochemistry* **2012**, *51*, 4237–4243. [CrossRef] [PubMed]
32. Cui, Y.; Wang, Y.; Tian, W.; Bu, Y.; Li, T.; Cui, X.; Zhu, T.; Li, R.; Wu, B. Development of a versatile and efficient C–N lyase platform for asymmetric hydroamination via computational enzyme redesign. *Nat. Catal.* **2021**, *4*, 364–373. [CrossRef]
33. Li, R.; Wijma, H.J.; Song, L.; Cui, Y.; Otzen, M.; Tian, Y.; Du, J.; Li, T.; Niu, D.; Chen, Y.; et al. Computational redesign of enzymes for regio- and enantioselective hydroamination. *Nat. Chem. Biol.* **2018**, *14*, 664–670. [CrossRef] [PubMed]

34. Liu, Z.; Yu, L.; Zhou, L.; Zhou, Z. One-pot biosynthesis of L-aspartate from maleate via an engineered strain containing a dual-enzyme system. *Appl. Environ. Microbiol.* **2019**, *85*, e01327-19. [CrossRef] [PubMed]
35. Fibriansah, G.; Veetil, V.P.; Poelarends, G.J.; Thunnissen, A.M.W.H. Structural basis for the catalytic mechanism of aspartate ammonia lyase. *Biochemistry* **2011**, *50*, 6053–6062. [CrossRef] [PubMed]
36. Gran-Scheuch, A.; Wijma, H.J.; Capra, N.; van Beek, H.L.; Trajkovic, M.; Baldenius, K.; Breuer, M.; Thunnissen, A.W.H.; Janssen, D.B. Bioinformatics and computationally supported redesign of aspartase for β-alanine synthesis by acrylic acid hydroamination. *ACS Catal.* **2025**, *15*, 928–938. [CrossRef] [PubMed]
37. Zhang, L.K.; Li, J.; Yu, L.Y.; Yan, Y.B.; Wu, H.C.; Tang, Y.P.; Li, Y.; Tang, B.C.; Ni, J.Z.; Qian, M.F.; et al. Nitrile Hydrolase and Its Application in β-Alanine Bioproduction. CN Patent CN115896078A, 4 April 2023.
38. Fan, W.; Wang, J.G.; Liang, Y.; Gao, S.L. Aspartate Ammonia Lyase Mutant and Its Application. CN Patent CN110791493B, 9 March 2021.
39. Liu, L.; Fan, Y.; Xia, D.D. Aspartase Mutant and Its Application. CN Patent CN116836963A, 3 October 2023.
40. Wu, B.; Liu, Y.; Li, R.F.; Zhang, D.Z.; Liu, Z.C.; Zhang, H. Aspartase Variants and Their Preparation Methods and Applications. CN Patent CN109385415B, 27 July 2021.
41. Xu, J.P.; Shi, S.M.; Bocola, M.; Cai, B.Q.; Chen, H.B. A Computational Method for Designing Protease Mutants with non-Natural Substrate Activity. CN Patent CN115295077A, 4 November 2022.
42. Qi, W.; You, S.; Liu, Y.; Sun, X.; Liu, Y.; Wang, Y.; Li, Y.; Zhang, X.; Wang, H.; Li, Z. Aspartase Mutants, Coding Genes, and Engineered Bacteria. CN Patent CN112725322A, 30 April 2021.
43. Wang, J.; Liang, Y.; Wei, Y.; Ren, L. Aspartase Mutant for Producing 3-Aminopropionitrile. CN Patent CN114934037B, 27 June 2023.

Disclaimer/Publisher's Note: The statements, opinions and data contained in all publications are solely those of the individual author(s) and contributor(s) and not of MDPI and/or the editor(s). MDPI and/or the editor(s) disclaim responsibility for any injury to people or property resulting from any ideas, methods, instructions or products referred to in the content.